Maturity sensors placement based on the temperature transitional boundaries

Ye.B. Utepov[1, 4], A. Aniskin[2], A.P. Ibrashov[3], A. Tulebekova[1]*
[1] *L.N. Gumilyov Eurasian National University, Nur-Sultan, Kazakhstan*
[2] *University North, Koprivnica, Croatia*
[3] *CSI Research & Lab, LLP, Nur-Sultan, Kazakhstan*
[4] *"NIISTROMPROJECT" LLP, Almaty, Kazakhstan*
* E–mail: utepov-elbek@mail.ru

Keywords: reinforced concrete, hydration, temperature, sensors, positioning, interpolation, heat map

Abstract. The way in which the maturity sensors are placed determines their number required for a particular monolithic building skeleton. Previous studies scarcely address this aspect, providing only logical assumptions. Therefore, this study proposes an alternative placement strategy for maturity sensors based on transitional boundaries of concrete curing temperature distribution. The transitional boundaries may be determined using the heat map representation of temperature distribution, where the unknown values are computed by the Inverse Distance Weighting method. Based on the experimentally poured concrete slab and randomly embedded maturity sensors revealed that the transitional boundaries form elliptical shapes. The temperature distributions along the largest diameter of ellipses were plot on a single graph, which created regular and reverse parabolas. As a result, the distance between the closest opposite intersections of the parabolas is assumed as the maximum acceptable step to set the maturity sensors. The proposed placement strategy may be applicable for the sensors that measure various continuous phenomena, for example the relative humidity.

1. Introduction

There are many methods to control the concrete compressive strength. Some of them are clustered as destructive, some as nondestructive [1]. The traditional destructive control of concrete strength is based on the tests of standard concrete specimens by compression using the press machines. In the field conditions the standard specimens are prepared from the freshly arrived concrete mixture in parallel with the pour of concrete structure. Usually for each batch of the concrete mixture, at least 9 specimens are prepared. It is supposed that the specimens cure at the same ambient conditions as the concrete structure. At the curing ages of 3, 7 and 28 the specimens are tested. Three specimens are tested at each testing day. The load of squeezing corresponding to the moment when the specimen starts breaking, or the cracks appear on it, is fixed as the value of the strength. The average of strengths of the three specimens is taken as a value of concrete compressive strength at a certain day of curing [2]. This method of strength control is widely accepted worldwide as the more robust method. However, due to several circumstances and human factor the testing procedure is not always precisely followed in the constructing sites. These circumstances may include wrong sequence and timing of the preparation of specimens (e.g. the structure is poured too late after the specimens are prepared), confusing the batch of concrete mixture, and the difference of curing conditions (e.g. after preparation the specimens are hold at the laboratory). Moreover, it is worth noting the difference of sizes between the specimens and a real structure. Massive structures cure slower than the smaller ones. All of this makes the test results more unreliable. Nevertheless, the method is still extensively used, since it is regulated by the actual construction standards of almost each country all over the world [1, 2]. The traditional nondestructive concrete-control mostly refers to the shock-impulse method implemented in a special equipment. The mechanism of shock-impulse method is based on the energy appearing at the hit of hammer of the corresponding equipment. According to the preliminary calibrations, the obtained energy is converted into the value of compressive strength. The shock-impulse method is also regulated by the construction standards in many countries. Its main advantage is that it gives the result immediately. The equipment is mostly portable and easy to

handle [3]. Although it has certain advantages, the method has its own disadvantages. The method enables obtaining the compressive strength at a certain point where the hammer hits. Therefore, referring the obtained value of compressive strength to the whole structure would be a wrong decision. Since in reality, every part of the structure cures differently. This is why the several points of the structure must be tested. In general, both traditional methods imply the human involvement, labor-intensive, cost-inefficient, and disable real time measurements [4].

The concrete curing refers to the exothermal process [5], where the cement hydration releases heat. This is why at early ages of concrete curing the internal temperature of concrete intensively increases and slowly decreases afterwards [6]. The continuous strength gain of the concrete throughout many years indicates that the chemical reaction in it is long-lasting. Measuring the internal temperature over time opens great opportunities during concrete works. It helps making proper decisions on unmolding the formwork and loading the structures, and influences the pace of construction [7]. This feature of concrete is studied in many previous works [6, 8–11]. It is proven that the combined effect of time and temperature enables estimating the actual compressive strength of the concrete. To refer to this effect, [12] introduced the terms «maturity index» or «temperature-time factor». There are two maturity functions, enabling concrete strength estimation: Nurse-Saul and Arrhenius functions. The Nurse-Saul function assumes that there is a linear relationship between the maturity and hydration temperature history. The Arrhenius function assumes that there is an exponential relationship between the compressive strength and hydration temperature [12]. The maturity method is effective by means of embedded temperature sensors that can be either wired or wireless in terms of control [13, 14]. The sensors enable continuous monitoring of internal parameters of concrete (not only the temperature) as long as they are powered by electricity [15–17]. The manufacturers of such sensors are the Canadian company «Giatec» [18, 19], American company «ConcreteSensors» [20] and some others are widely discussed in [5]. The advantages and disadvantages of these sensors are thoroughly discussed by [21], who proposed the less expensive sensor prototype with improved features (Figure 1).

Figure 1. Sensor prototype [21].

In [21] it is argued that the economic impact for construction sites may be reached due to the timely knowledge about the concrete strength, which saves overhead expenses. However, using too many sensors is quite costly [5]. Because the expenses to purchase many sensors may leave no savings at all. Therefore, it is important to define a necessary number of sensors to be used for a certain monolithic building skeleton in advance. The number of sensors needed depend on the location where the sensors must be installed. Currently, the optimal location of the concrete maturity sensors has not been well studied, but there are studies on optimal placement strategies of other types of sensors [22–24], mainly used for modal tests [25] proposed the sensor placement strategy based on the finite element simulations, where the case of heat transfer problem in the concrete slab was considered. Due to the specificity of the internal temperature behavior of concrete curing, none of the considered above strategies seems appropriate for maturity sensor placement. However, some techniques proposed by [25], such as representing the heat transfer in a colored heat map, may be helpful [26] suggests to consider three aspects when selecting the installation locations of the concrete maturity sensors, such as critical weather locations on the structural element, concrete mixture pour schedule, and the structurally critical locations. The environmental phenomena, such as wind, rain, and shadow may influence the internal temperature of concrete to some extent, which eventually affects its strength gain [21] proposed a cross-correlation matrix that shows how the concrete parameters influence each other at laboratory and field conditions. According to this matrix for the studied mixture, in the ambient conditions the effect of internal temperature on the strength gain is only 14 %. The rest of 86 % goes to the ambient temperature (33 %), internal relative humidity (25 %) and ambient relative humidity (29 %). The pour schedule is also important. Since one huge structure may require several pours until it is filled completely, and the interval between the pours may fluctuate up to several hours. In this case [26] proposes a mandatory installation of the sensor in the location of the last pour. Due to the concrete at this location will most likely gain the necessary strength later than the concrete at the previously poured locations. Probably the most important locations to install the sensors are the critical locations, where the highest negative and positive

Утепов Е.Б., Анискин А., Ибрашов А., Тулебекова А.

design moments are observed. Commonly, in the monolithic building skeleton the maximum positive moment is located at a mid-span, and a maximum negative moment is located at a slab-column boundary. These locations are considered the most responsible when conducting the design of spatial skeleton of the building [26]. Other aspects that need to be considered are the power of the network (if the sensor is wireless) and the safety from accidental damage. The existing analogs of maturity sensors [18, 20] use Bluetooth data transfer protocol. Because of the short operating distance of Bluetooth, it is important to install the sensors at easy-accessible locations, to ease the future data retrieval. To eliminate this shortcoming, [21] proposed to change the Bluetooth into the Narrow Band IoT network. The safe locations to install the sensors would be those with low workers traffic. The concrete pouring may also damage the sensors. Therefore, it is necessary to install them in a distance from the pouring location [26].

Previous studies propose only logically assumed locations to install the sensors without providing justifications. Considering the importance of the sensor positioning, current study proposes an alternative approach for allocation of the embedded sensors. As per [27], the temperature is a continuous phenomenon. This means its values change smoothly throughout the surface until the border (hereinafter – transitional boundary) where the influence of other phenomena begins to prevail. If considering the internal temperature during the concrete curing process, the same behavior may be observed. This study anticipates that such behavior of the internal temperature of concrete gives understanding of at which step the maturity sensors must be set. Hypothesized that the transitional boundaries most likely occur around the reference points, where the values of the temperature are known, and creates elliptical shapes. Therefore, it is assumed that the maximum setting step of maturity sensors must be less than the largest diameter of each elliptical shape of transitional boundary. The suitable approach to define and measure the transitional boundaries could be the colored heat map representation of temperature distribution as used in [25], which enables visualizing the change over the surface somewhat clearly. In the light of the aforementioned assumptions, this study aims to develop and justify an alternative strategy of concrete maturity sensor placement. Thus, the concrete curing temperature distribution is considered as the object of study and the transitional boundaries of temperature values – as the subject of study. Further chapters enclose the proposed hypothesis more in detail based on the experimental studies conducted.

2. Methods

To create the heat maps of temperature distribution and determine the transitional boundaries, at least the values of temperature at the reference points must be predefined. The rest of temperature values throughout the whole surface can be determined using the interpolation technique. Laying out all the temperature values at the corresponding positions in the 2D plane and assigning scaled colors to them generates a heat map. Moreover, the more reference points involved, the more precisely the interpolation calculates the temperatures at each position in the plane. To avoid unrealism, the reference points must be randomly distributed across the plane. The heat map may give a proper justification of the maximum setting step of maturity sensors. To investigate the hypothesis, a reinforced concrete slab experimentally taken as the 2D plane. The slab had the rectangular shape with the dimensions of 12×6×0.2 m and poured outdoor. Conducted the following sequence of operations:

1) Before the pour of the slab by the concrete, 5 maturity sensors developed by [21] were mounted on the rebar of the slab in random locations in the plane, as shown in the Figure 2 below. The sensors were located in the center of the slab thickness.
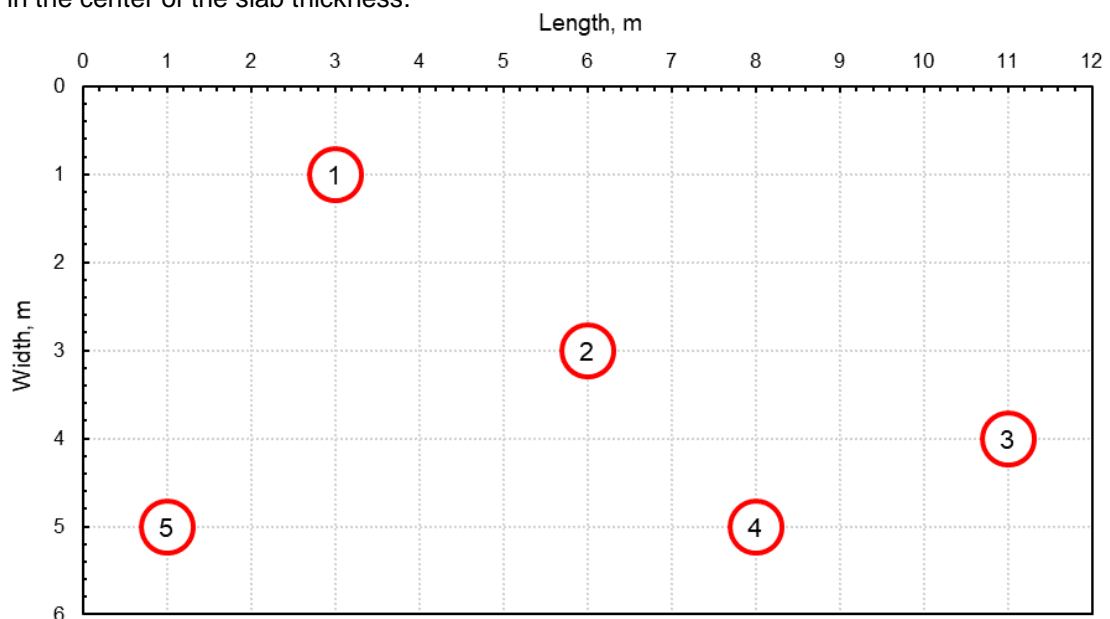

Figure 2. Locations of the maturity sensors.

Utepov, Ye.B., Aniskin, A., Ibrashov, A.P., Tulebekova, A.

2) The slap was poured by the concrete B25 M350 in 6 approaches of a skip by around 14 m^3 of concrete mixture from one batch. Total time spent for the pouring process was less than an hour. The ambient temperature was between 10÷12 °C. The slab had no thermal insulation. The particleboard was used as a formwork of the slab. The thermos-physical properties of the formwork were not considered, since it was expected that its effect would be insignificant due to the similarity of the ambient temperature and the initial temperature of the concrete mixture.

3) Immediately after the pour, with the interval of one hour the sensors measured the internal temperature of concrete for 28 days (i.e. each sensor had 672 readings).

4) The readings of each sensor were transferred to the computer and converted into Excel format.

5) In the Excel document, 672 sheets were created, each containing the readings of corresponding hour of measurements.

6) In each sheet, 2D planes were created with the size of 1200×600 cells (i.e. the size of each cell was equivalent to 10×10 cm in regard to the size of the concrete slab). The values of temperature at reference points (existing readings) were laid in the corresponding cells of each of the planes (Figure 2).

7) The unknown values of temperature in the 2D planes were interpolated using the Inverse Distance Weighting (IDW) method. IDW is a spatial interpolation method that enables estimating the unknown values based on the weighted average of the known values [28, 29]. Thus, each cell on the 2D plane was assigned by the equation, where the weights represented the distances from each cell to the locations of reference points. The equation is as followed:

$$t_c = \frac{\sum\limits_{i=1}^{n} \dfrac{t_i}{d_i^p}}{\sum\limits_{i=1}^{n} \dfrac{1}{d_i^p}}, \tag{1}$$

where t_c is unknown value of temperature in the cell;

i is number of reference point;

t_i is known value of temperature at the reference point i;

d_i is search distance from the cell to the reference point i;

p is power of IDW (p = 2) [29].

8) To generate the hourly heat maps, the cells on the 2D plane were color-scaled using the Excel conditional formatting feature based on the values of temperature that the cells contained. The choice of Excel to create heat maps is justified by its flexibility in the implementation of custom method for estimating unknown values of temperature based on existing ones. Existing software to estimate temperature field are adapted to solve specific tasks such as thermal design. They are based on certain methods, which cannot be customized and do not cover the needs of this study. Thereby, they considered the influence of ambient temperature on a particular object, which temperature is initially stable. In case of concrete mixture, its temperature is instable and fluctuating over time. Moreover, there is no need to consider the ambient temperature when the sensors measure the actual internal temperature of concrete.

9) All the hourly heat maps were combined into one average in order to define the averaged transitional boundaries and the shaded elliptical shapes that they surround. Then there were drawn the cross-section lines passing through the reference points and coinciding in the orientation of the largest diameters of elliptical shadings.

10) Temperature distribution graphs were created in the cross-sections, and the distance between the opposite intersections of the graphs enabled determining the acceptable setting step of sensors.

3. Results and Discussion

As planned, the measurement of temperature in the body of reinforced concrete slab was carried out by the embedded sensors for 28 days with the interval of 1-hour. The sensors collected 672 readings each. When displaying all the obtained readings onto the chart, observed the following behavior of the concrete curing temperature presented in Figure 3 below.
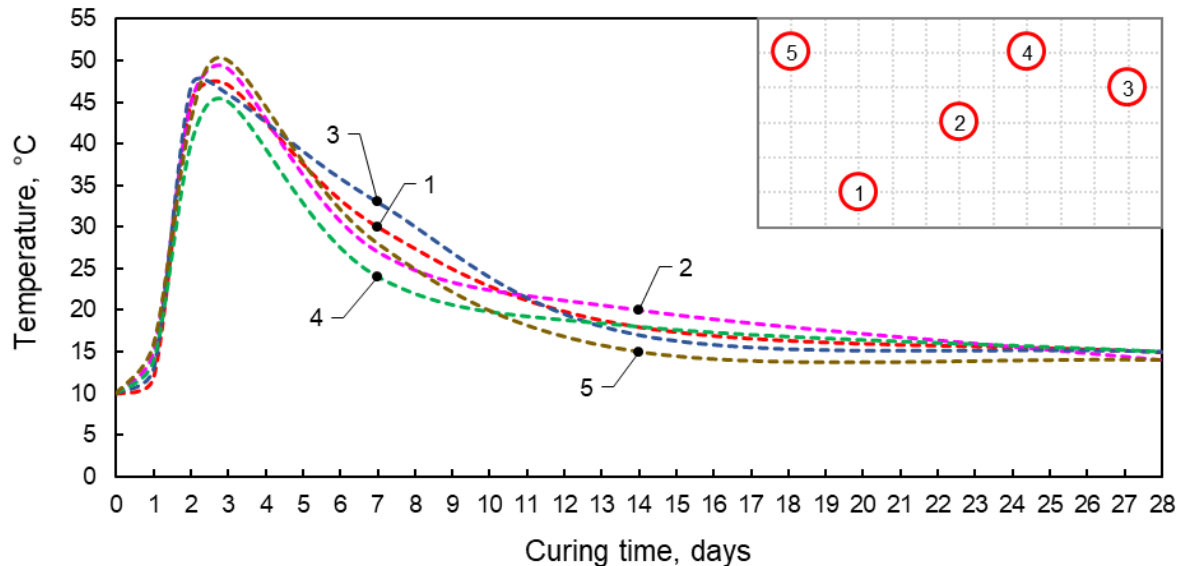
Figure 3. Temperature mode of concrete curing.

From the figure above it is seen that although the initial temperature of concrete mixture when pouring was uniform (around 10 °C), at further concrete curing observed the difference between the values of temperature at all reference points (i.e. sensor locations). This indicates that the concrete gained its strength unevenly throughout the whole period. Some parts of the slab gained strength faster than other parts. There could be many reasons of this consequence, such as poor quality of concrete mixture and its rheological structure, influence of environmental phenomena or simply human error while taking care of the concrete. However, it is impossible to achieve a perfectly even curing of concrete, especially when it comes to the extended and flat structures. In general, it is shown that at the second and third days the internal temperature reached its peak. This is due to the exothermal reaction during the cement hydration. Thus, the highest temperature of 50 °C reached on the third day at the location of sensor Nomber 5. Little earlier, on the second day the temperature at the location of sensor No. 3 reached its peak at 47 °C. The temperature peak at other sensor locations fluctuated between 45–49 °C. The notable variation of the temperature between 24–33 °C is observed on the 7th day, which is probably most like is caused by the influence of external phenomena. Furthermore, the temperatures at the sensor locations smoothly decreased up to the 28th day and reached the ambient temperature of around 14–15 °C. The small variation of temperature at the 28th day may indicate that the strength of concrete at all the reference points became more or less uniform.

To enable smooth transition of scaled colors in the heat maps, the 2D plane was split into the grid of cells with the size of 10 cm. A smaller cell size, such as 1 cm, would make the transition even smoother. Thus, 672 heat maps were obtained for each hour within 28 days. The heat maps of the most important ages of 1, 2, 3, 7, 14 and 28 days of the concrete curing are presented in Figure 4 a), b), c), d), e) and f) respectively.

The figures above demonstrate how the temperature changed during the 28 days of concrete curing. The heat maps were generated based on the values of temperature at each cell of 2D planes. Here some values were known (at reference points), some were unknown and interpolated using IDW method, as planned. The heat maps used three scaled colors to demonstrate the change of the temperature values on the plane: blue, white and red. The cells colored in blue and red represents the lower and the higher values of temperature respectively. The white color is selected to indicate the transitional boundaries between the lower and higher values of temperature and vice versa. It should be noted that the scale of the colors at each heat map of a certain period is assigned between the lowest and the highest values of temperature within the corresponding heat map. For note, if scaling the colors between the lowest and highest values of temperature within the whole period of 28 days of concrete curing (e.g. between 10–50 °C), the change of the temperature values in majority of heat maps would be indistinguishable. The obtained heat maps colorfully emphasize the dynamics of changes in the internal temperature of concrete, which can eventually provoke a variation in the strength gain in different parts of the concrete structure. In this regard, it helps better understanding the hydration reaction in the concrete structure to make proper decisions on preventive measures.

To gain a general picture on the reasonable setting step of the sensors, the average heat map were generated based on the values of temperature at all the cells of all 672 hourly heat maps. The resulting heat map is shown in Figure 5 below.
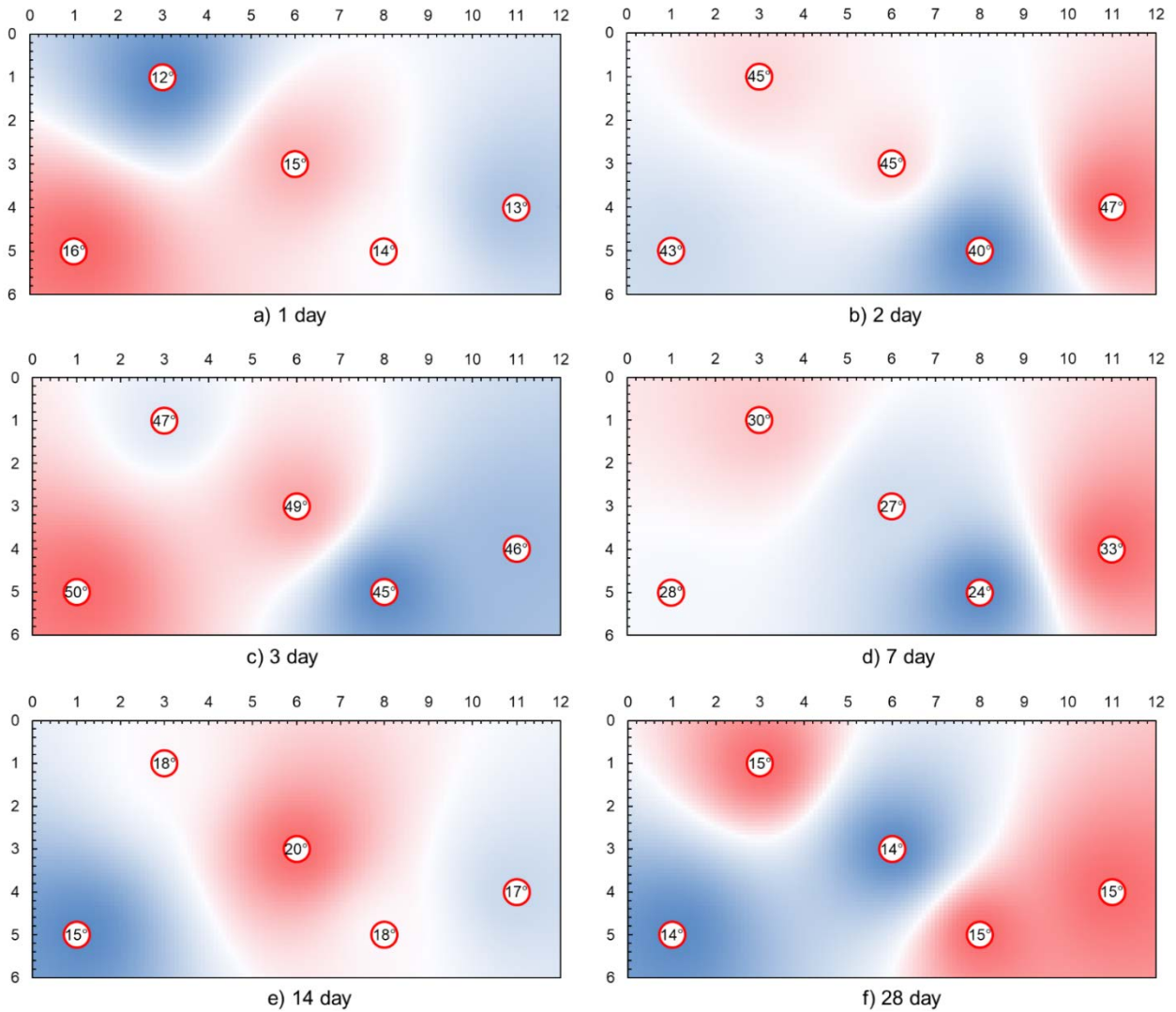
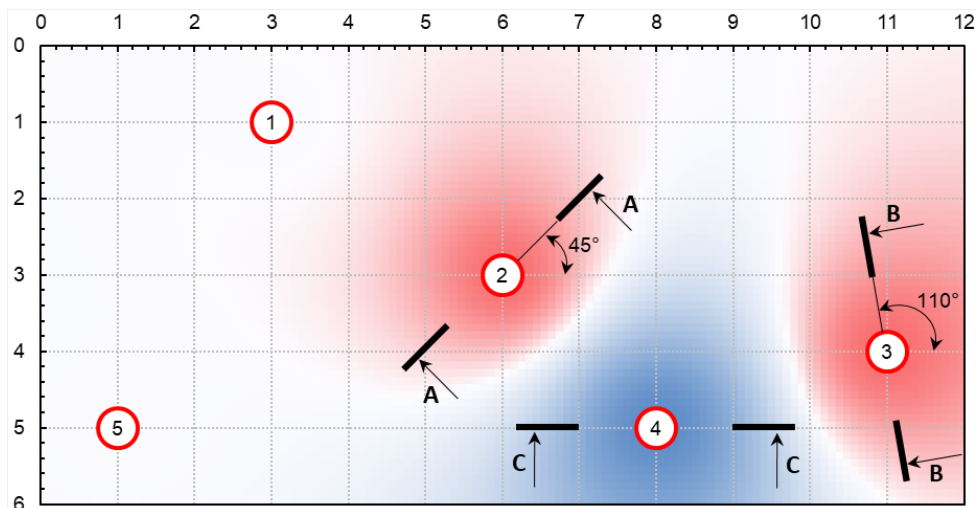**Figure 4. Heat maps of temperature distribution.**

Figure 5. Heat map of average temperature distribution.

The obtained heat map depicted distinct shadings with ellipsis shapes around three reference points. Here the lowest temperature values in the cells colored in blue are observed around the sensor No. 4 and the highest – around the sensors No. 2 and 3 in the cells colored in red. Other sensor locations fell on to the mean values of the temperature distribution. Such a picture is a consequence of higher instability of the values of internal temperature at the reference points No. 2, 3 and 4, than at the reference points No. 1 and 4, based on the readings during 28 days of concrete curing. However, it is this picture that gives basis for further reasoning and justification of the acceptable sensor setting step. Thereby, according to the last operation of this study, the temperature distribution graphs were created at the cross-sections A-A, B-B and C-C that pass

through the reference points. For the location of sensor No. 2, 3 and 4, the cross-sections were selected at the angles of 45, 110 and 0 degrees to the horizontal axis respectively, and the graphs of temperature distribution were draw, as presented in Figure 6 below.
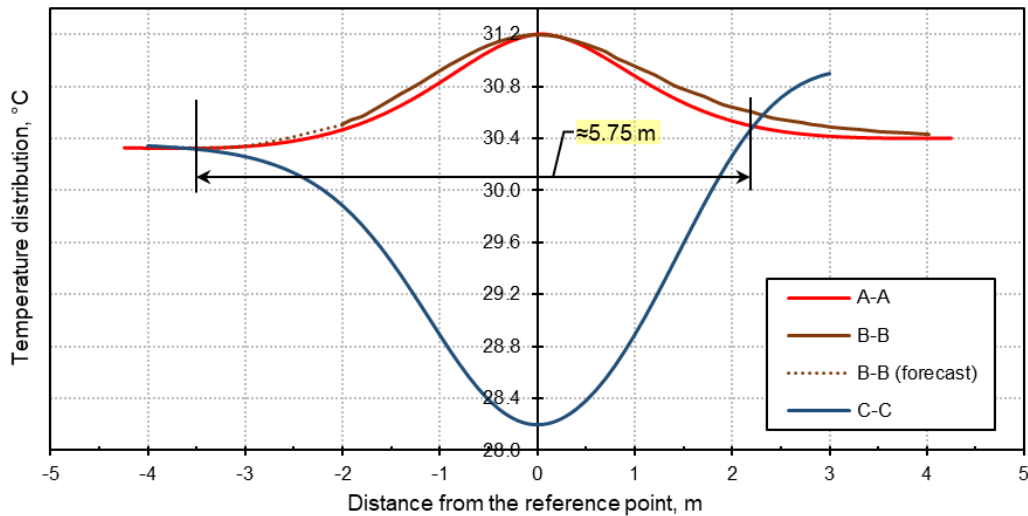

Figure 6. Distribution of temperature at cross-sections.

From the figure above it is seen that the values of temperature at cross-sections fell within the range of 28.2–31.2 °C. The graphs took a parabolic shape with the peaks on the vertical axis. The higher peaks are observed at the reverse parabolic graphs A-A and B-B, where the highest values of temperature was identified (Figure 5). Conversely, the lower peak is observed at the regular parabolic graph C-C. Since the lower part of the cross-section B-B rests close on the border of the 2D plane, its temperature distribution graph was prolonged through the forecast of its trend (marked with dotted line), in order to enable its intersection with the graph C-C having the lower peak. If considering the graphs A-A and B-B, it may be noticed that their transitional boundaries start in an average distance of 3.5 m from their reference points. In case of the graph C-C, from one side (left) the transitional boundary starts in a distance of 4 m, while from the other side (right), it starts in a distance of 3 m from the reference point. To retrieve the combined effect of all the temperature distribution graphs, suggested to pay attention onto the intersection of the graphs on both sides. Such intersections may create several new asymmetrical shapes, depending on the number of cross-sections taken. Proposed that the distance between the closest opposite intersections of the temperature distribution graphs represented by regular and reverse parabolas may be considered as the maximum acceptable setting step of maturity sensors. In addition, to ease the selection of the intersections, proposed to consider the asymmetrical shape with the smallest area that lays more inward compared to other asymmetrical shapes. This study revealed the distance of 5.75 m between the two opposite intersections of the temperature distribution graphs, based on three considered cross-sections. Thus, the setting step of maturity sensors suggested to be set less than this distance.

Similar results may be obtained if using a thermal imaging camera instead of the maturity sensor. However, it should be noted that the thermal imaging camera enable reading the temperature only on the surface of concrete structure, and therefore this equipment is not appropriate to replicate this study. It is important to have the readings of internal temperature of concrete structure. Current study involved the wireless maturity sensors. However, to replicate the study one may use wired temperature sensors as well.

4. Conclusion

1. Previous studies proved the effectiveness of the embedded maturity sensors for monitoring the reinforced concrete structures compared to the traditional destructive and nondestructive methods in terms of labor-intensity, portability and comfortableness, as well as ability of real time measurements. However, the cost-efficiency of the embedded sensors depends on their number used for a certain volume of concrete structure or the whole building skeleton due to their relatively high purchase price. Therefore, it is worth paying particular attention to the way the sensors are placed in the concrete structure when using them. Since the more efficient the positioning of the sensors, the less they can be used.

2. It is revealed that the existing methods to establish locations of concrete maturity sensors are weakly substantiated and based solely on logical assumptions, not considering the possible variation of curing intensity at different parts of the concrete structure. Therefore, in this study proposed the alternative method to position the maturity sensors underpinned by the dynamics of transitional boundaries of temperature distribution during the whole concrete curing period.

3. Experimentally identified that the transitional boundaries surround the patterns with more or less similar (or clustered) values of temperature. Moreover, these patterns most likely have the elliptical shapes.

The temperature distribution throughout the whole dimension of concrete structure may be obtained using the Inverse Distance Weighting interpolation method, using the known values from the sensor measurements and their locations. Thereby, in current study defined the convenience of heat map representation to clearly demonstrate the transitional boundaries and the pattern of temperature distribution. The heat map enables expressing the patterns by the color-scaled shadings of each point at the concrete structure, where the intensity of the colors are dependent of the values of temperature at the points. It was established that the suitable color scheme of the heat maps may consist of three different colors, that correspond to the values of low, medium and high temperatures on a certain heat map. In this study selected the color scheme that consists of blue, white and red colors. In this study 672 hourly heat maps were created that give clear visual interpretation of the dynamics of temperature distribution throughout the 28-day period. To enable defining their combined effect, it is proposed to create the consolidated heat map, based on the sum of values of all the heat maps at each respective points.

4. The study identified that the combined plotting of temperature distribution along the lines that coincide with the direction of the largest diameter of formed in the consolidated heat map elliptical shadings creates the asymmetrical shapes. These shapes are composed of the regular and reverse parabolas. Depending on the number of shadings selected to the plot, there may occur several asymmetrical shapes. It is suggested to consider the distance between the intersection of regular and reverse parabolas that create the asymmetrical shape with the smallest area as the maximum acceptable setting step of the maturity sensors. As a result of the experiments conducted, it is not recommended to exceed the setting step of the maturity sensor above 5.75 m.

5. Acknowledgements

References

1. Kibar, H., Ozturk, T. Determination of concrete quality with destructive and non-destructive methods. Computers and Concrete [Online]. 2015. 15(3). Pp. 473–484. DOI: 10.12989/cac.2015.15.3.473. URL: http://koreascience.or.kr/journal/view.jsp?kj=KJKHDQ&py=2015&vnc=v15n3&sp=473

2. Malek, J., Kaouther, M. Destructive and non-destructive testing of concrete structures [Online]. Jordan Journal of Civil Engineering. 2014. 8(4). Pp. 432–441. URL: https://pdfs.semanticscholar.org/75e7/564faf6e1f4e83a0d73a3418236df16515d2.pdf

3. Erdal, H., Erdal, M., Simsek, O., Erdal, H.I. Prediction of concrete compressive strength using non-destructive test results. Computers and Concrete. 2018. 21(4). Pp. 407–417. DOI: 10.12989/cac.2018.21.4.407.

4. Helal, J., Sofi, M., Mendis, P. Non-destructive testing of concrete: A review of methods [Online]. Electronic Journal of Structural Engineering. 2015. 14(1). Pp. 97–105. URL: http://www.ejse.org/Archives/Fulltext/2015-1/2015-1-9.pdf

5. Taheri, S. A review on five key sensors for monitoring of concrete structures [Online]. Construction and Building Materials. 2019. 204. Pp. 492–509. DOI: 10.1016/j.conbuildmat.2019.01.172. URL: https://linkinghub.elsevier.com/retrieve/pii/S0950061819302090

6. Ge, Z., Wang, K. Modified heat of hydration and strength models for concrete containing fly ash and slag [Online]. Computers & concrete. 2009. 6(1). Pp. 19–40. DOI: 10.12989/cac.2009.6.1.019. URL: http://koreascience.or.kr/journal/view.jsp?kj=KJKHDQ&py=2009&vnc=v6n1&sp=19

7. Zemajtis, Je.Z. Role of Concrete Curing. Portland Cement Association. Skokie, 2014.

8. Anwar Hossain, K.M. Influence of extreme curing conditions on compressive strength and pulse velocity of lightweight pumice concrete [Online]. Computers & concrete. 2009. 6(6). Pp. 437–450. DOI: 10.12989/cac.2009.6.6.437. URL: http://koreascience.or.kr/journal/view.jsp?kj=KJKHDQ&py=2009&vnc=v6n6&sp=437

9. Chen, H.-J., Yang, T.-Y., Tang, C.-W. Strength and durability of concrete in hot spring environments [Online]. Computers & concrete. 2009. 6(4). Pp. 269–280. DOI: 10.12989/cac.2009.6.4.269. URL: http://koreascience.or.kr/journal/view.jsp?kj=KJKHDQ&py=2009&vnc=v6n4&sp=269

10. Zhang, B., Cullen, M., Kilpatrick, T. Spalling of heated high performance concrete due to thermal and hygric gradients [Online]. Advances in concrete construction. 2016. 4(1). Pp. 1–14. DOI: 10.12989/acc.2016.4.1.001. URL: http://koreascience.or.kr/journal/view.jsp?kj=TPTPR5&py=2016&vnc=v4n1&sp=1

11. Farzampour, A. Temperature and humidity effects on behavior of grouts. Advances in concrete construction. An international journal. 2017. 5(6). Pp. 659–669. DOI: 10.12989/acc.2017.5.6.659.

12. ASTM C1074. Standard Practice for Estimating Concrete Strength by the Maturity Method, West Conshohocken, Pennsylvania, USA, 1998.

13. Lee, H.-S., Cho, M.-W., Yang, H.-M., Lee, S.-B., Park, W.-J. Curing Management of Early-age Concrete at Construction Site using Integrated Wireless Sensors [Online]. Journal of Advanced Concrete Technology. 2014. 12(3). Pp. 91–100. DOI: 10.3151/jact.12.91_100. URL: https://www.jstage.jst.go.jp/article/jact/12/3/12_91/_article

14. Kwon, S.H., Jang, K.P., Bang, J.-W., Lee, J.H., Kim, Y.Y. Prediction of concrete compressive strength considering humidity and temperature in the construction of nuclear power plants [Online]. Nuclear Engineering and Design. 2014. 275. Pp. 23–29. DOI: 10.1016/j.nucengdes.2014.04.025. URL: https://linkinghub.elsevier.com/retrieve/pii/S0029549314002507

15. Ashteyat, A.M., Ismeik, M. Predicting residual compressive strength of self-compacted concrete under various temperatures and relative humidity conditions by artificial neural networks. Computers and Concrete. 2018. 21(1). Pp. 47–54. DOI: 10.12989/cac.2018.21.1.047.

16. Hannan, M.A., Hassan, K., Jern, K.P. A review on sensors and systems in structural health monitoring: Current issues and challenges. Smart Structures and Systems. 2018. 22(5). Pp. 509–525. DOI: 10.12989/sss.2018.22.5.509.

Утепов Е.Б., Анискин А., Ибрашов А., Тулебекова А.

17. Ranz, J., Aparicio, S., Fuente, J.V., Anaya, J.J., Hernández, M.G. Monitoring of the curing process in precast concrete slabs: An experimental study [Online]. Construction and Building Materials. 2016. 122. Pp. 406–416. DOI: 10.1016/j.conbuildmat.2016.06.041. URL: https://linkinghub.elsevier.com/retrieve/pii/S0950061816309680

18. Walsh, D. IoT Hero from Giatec Develops «SmartRocks» with Bluetooth [Online]. URL: https://www.silabs.com/community /blog.entry.html/2016/01/18/iot_hero_from_giatec-Av1P (date of application: 25.08.2019).

19. Giatec, S. Real-time temperature and maturity monitoring of concrete [Online]. URL: https://www.giatecscientific.com/pro ducts/concrete-sensors/smartrock-maturity-meter/ (date of application: 25.08.2019).

20. ConcreteSensors. Durable wireless concrete sensor for concrete strength, temperature, RH [Online]. URL: https://concret esensors.com/concrete-strength-and-temperature-monitoring-platform/wireless-concrete-sensor/ (reference date: 25.08.2019).

21. Utepov, Y.B., Khudaibergenov, O.A., Kabdush, Y.B., Kazkeev, A.B. Prototyping an embedded wireless sensor for monitoring reinforced concrete structures. Computers and Concrete. 2019. 24(2). Pp. 95–102. DOI: 10.12989/cac.2019.24.2.095.

22. Liu, K., Yan, R.-J., Guedes Soares, C. Optimal sensor placement and assessment for modal identification [Online]. Ocean Engineering. 2018. 165. Pp. 209–220. DOI: 10.1016/j.oceaneng.2018.07.034. URL: https://linkinghub.elsevier.com/retrieve/pii/S00 29801818305584

23. Yin, H., Dong, K., Pan, A., Peng, Z., Jiang, Z., Li, S. Optimal sensor placement based on relaxation sequential algorithm [Online]. Neurocomputing. 2019. 344. Pp. 28–36. DOI: 10.1016/j.neucom.2018.03.088. URL: https://linkinghub.elsevier.com/retrieve /pii/S0925231219301742

24. Zhang, J., Maes, K., De Roeck, G., Reynders, E., Papadimitriou, C., Lombaert, G. Optimal sensor placement for multi-setup modal analysis of structures [Online]. Journal of Sound and Vibration. 2017. 401. Pp. 214–232. DOI: 10.1016/j.jsv.2017.04.041. URL: https://linkinghub.elsevier.com/retrieve/pii/S0022460X1730370X

25. Nath, P., Hu, Z., Mahadevan, S. Sensor placement for calibration of spatially varying model parameters [Online]. Journal of Computational Physics. 2017. 343. Pp. 150–169. DOI: 10.1016/j.jcp.2017.04.033. URL: https://linkinghub.elsevier.com/retrieve /pii/S0021999117303042

26. Giatec, S. Practical Installation Applications for Wireless Maturity Sensors [Online]. URL: https://www.giatecscientific.com /education/practical-installation-applications-for-wireless-maturity-sensors/ (reference date: 25.08.2019).

27. Kessler, F.C., Battersby, S.E. Working with Map Projections: A Guide to Their Selection. CRC Press, 2019. Pp. 65.

28. Jing, M., Wu, J. Fast image interpolation using directional inverse distance weighting for real-time applications [Online]. Optics Communications. 2013. 286. Pp. 111–116. DOI: 10.1016/j.optcom.2012.09.011. URL: https://linkinghub.elsevier.com/retrieve/ pii/S0030401812009595

29. GISGeography. Inverse Distance Weighting (IDW) Interpolation [Online]. URL: https://gisgeography.com/inverse-distance-weighting-idw-interpolation/ (date of application: 25.08.2019).

Contacts:

Yelbek Utepov, +7(700)2101733; utepov-elbek@mail.ru

Aleksej Aniskin, +3(8592)304-94-06; aaniskin@unin.hr

Azamat Ibrashov, +7(701)7676673; a.ibrashov@csi.kz

Assel Tulebekova, +7(701)6481866; krasavka5@mail.ru

Размещение датчиков зрелости в зависимости от границ температурного перехода

Е.Б. Утепов[1, 4]*, А. Анискин[2], А. Ибрашов[3], А. Тулебекова[1]

[1] Евразийский национальный университет им. Л.Н. Гумилева, Нур-Султан, Казахстан,

[2] Университет Север, Копривница, Хорватия,

[3] ТОО CSI Research & Lab, Нур-Султан, Казахстан,

[4] ТОО "НИИСТРОМПРОЕКТ", Алматы, Казахстан

* E-mail: utepov-elbek@mail.ru

Ключевые слова: железобетон, гидратация, температура, датчики, размещение, интерполяция, тепловая карта

Аннотация. От способа размещения датчиков зрелости зависит их количество, необходимое для определенного каркаса монолитного здания. Прежние исследования слабо освящают данный аспект, приводя лишь логические предположения. Поэтому в данном исследовании предлагается альтернативная стратегия размещения датчиков, основанная на переходных границах распределения температуры твердения бетона. Переходные границы могут быть определены с помощью построения тепловой карты распределения температуры, где неизвестные значения рассчитываются методом обратного взвешивания расстояния. На основе экспериментально залитой бетонной плиты с произвольно встроенными датчиками зрелости установлено, что переходные границы образуют эллиптические формы. Распределение температур по наибольшему диаметру эллипсов было нанесено на график, что привело к созданию правильных и обратных парабол. В результате, расстояние между ближайшими противоположными точками пересечения парабол принято в качестве максимально допустимого шага для установки датчиков зрелости. Предлагаемая стратегия размещения может быть применима к датчикам, которые измеряют различные непрерывные явления, например, относительную влажность.

Литература

1. Kibar H., Ozturk T. Determination of concrete quality with destructive and non-destructive methods // Computers and Concrete. 2015. № 3(15). Pp. 473–484. DOI:10.12989/cac.2015.15.3.473.

2. Malek J., Kaouther M. Destructive and non-destructive testing of concrete structures // Jordan Journal of Civil Engineering. 2014. № 4(8). Pp. 432–441.

3. Erdal H., Erdal M., Simsek O., Erdal H.I. Prediction of concrete compressive strength using non-destructive test results // Computers and Concrete. 2018. № 4(21). Pp. 407–417. DOI:10.12989/cac.2018.21.4.407.

4. Helal J., Sofi M., Mendis P. Non-destructive testing of concrete: A review of methods // Electronic Journal of Structural Engineering. 2015. № 1(14). Pp. 97–105.

5. Taheri S. A review on five key sensors for monitoring of concrete structures // Construction and Building Materials. 2019. № 204. Pp. 492–509. DOI:10.1016/j.conbuildmat.2019.01.172.

6. Ge Z., Wang K. Modified heat of hydration and strength models for concrete containing fly ash and slag. Computers & concrete. 2009. № 1(6). Pp. 19–40. DOI:10.12989/cac.2009.6.1.019.

7. Zemajtis J.Z. Role of Concrete Curing. Portland Cement Association. Skokie, 2014.

8. Anwar Hossain K.M. Influence of extreme curing conditions on compressive strength and pulse velocity of lightweight pumice concrete // Computers & concrete. 2009. № 6(6). Pp. 437–450. DOI:10.12989/cac.2009.6.6.437.

9. Chen H.-J., Yang T.-Y., Tang C.-W. Strength and durability of concrete in hot spring environments // Computers & concrete. 2009. № 4(6). Pp. 269–280. DOI:10.12989/cac.2009.6.4.269.

10. Zhang B., Cullen M., Kilpatrick T. Spalling of heated high performance concrete due to thermal and hygric gradients // Advances in concrete construction. 2016. № 1(4). Pp. 1–14. DOI:10.12989/acc.2016.4.1.001.

11. Farzampour A. Temperature and humidity effects on behavior of grouts // Advances in concrete construction, An international journal. 2017. № 5(6). Pp. 659–669. DOI:10.12989/acc.2017.5.6.659.

12. ASTM C1074. Standard Practice for Estimating Concrete Strength by the Maturity Method, West Conshohocken, Pennsylvania, USA, 1998.

13. Lee H.-S., Cho M.-W., Yang H.-M., Lee S.-B., Park W.-J. Curing Management of Early-age Concrete at Construction Site using Integrated Wireless Sensors // Journal of Advanced Concrete Technology. 2014. № 3(12). Pp. 91–100. DOI:10.3151/jact.12.91_100.

14. Kwon S.H., Jang K.P., Bang J.-W., Lee J.H., Kim Y.Y. Prediction of concrete compressive strength considering humidity and temperature in the construction of nuclear power plants // Nuclear Engineering and Design. 2014. № 275. Pp. 23–29. DOI: 10.1016/j.nucengdes.2014.04.025.

15. Ashteyat A.M., Ismeik M. Predicting residual compressive strength of self-compacted concrete under various temperatures and relative humidity conditions by artificial neural networks // Computers and Concrete. 2018. № 1(21). Pp. 47–54. DOI:10.12989/cac.2018.21.1.047.

16. Hannan M.A., Hassan K., Jern K.P. A review on sensors and systems in structural health monitoring: Current issues and challenges // Smart Structures and Systems. 2018. № 5(22). Pp. 509–525. DOI:10.12989/sss.2018.22.5.509.

17. Ranz J., Aparicio S., Fuente J.V., Anaya J.J., Hernández M.G. Monitoring of the curing process in precast concrete slabs: An experimental study // Construction and Building Materials. 2016. № 122. Pp. 406–416. DOI: 10.1016/j.conbuildmat.2016.06.041.

18. Walsh D. IoT Hero from Giatec Develops "SmartRocks" with Bluetooth. [Электронный ресурс]. URL: https://www.silabs.com/community/blog.entry.html/2016/01/18/iot_hero_from_giatec-Av1P (дата обращения: 25.08.2019).

19. Giatec, S. Real-time temperature and maturity monitoring of concrete. [Электронный ресурс]. URL: https://www.giatecscientific.com/products/concrete-sensors/smartrock-maturity-meter/ (дата обращения: 25.08.2019).

20. ConcreteSensors. Durable wireless concrete sensor for concrete strength, temperature, RH. [Электронный ресурс]. URL: https://concretesensors.com/concrete-strength-and-temperature-monitoring-platform/wireless-concrete-sensor/ (дата обращения: 25.08.2019).

21. Utepov Y.B., Khudaibergenov O.A., Kabdush Y.B., Kazkeev A.B. Prototyping an embedded wireless sensor for monitoring reinforced concrete structures // Computers and Concrete. 2019. № 2(24). Pp. 95–102. DOI:10.12989/cac.2019.24.2.095.

22. Liu K., Yan R.-J., Guedes Soares C. Optimal sensor placement and assessment for modal identification // Ocean Engineering. 2018. № 165. Pp. 209–220. DOI: 10.1016/j.oceaneng.2018.07.034.

23. Yin H., Dong K., Pan A., Peng Z., Jiang Z., Li S. Optimal sensor placement based on relaxation sequential algorithm // Neurocomputing. 2019. № 344. Pp. 28–36. DOI: 10.1016/j.neucom.2018.03.088.

24. Zhang J., Maes K., De Roeck G., Reynders E., Papadimitriou C., Lombaert G. Optimal sensor placement for multi-setup modal analysis of structures // Journal of Sound and Vibration. 2017. № 401. Pp. 214–232. DOI: 10.1016/j.jsv.2017.04.041.

25. Nath P., Hu Z., Mahadevan S. Sensor placement for calibration of spatially varying model parameters // Journal of Computational Physics. 2017. № 343. Pp. 150–169. DOI: 10.1016/j.jcp.2017.04.033.

26. Giatec S. Practical Installation Applications for Wireless Maturity Sensors. [Электронный ресурс]. URL: https://www.giatecscientific.com/education/practical-installation-applications-for-wireless-maturity-sensors/ (дата обращения: 25.08.2019).

27. Kessler F.C., Battersby S.E. Working with Map Projections: A Guide to Their Selection. CRC Press, 2019. Pp. 65.

28. Jing M., Wu J. Fast image interpolation using directional inverse distance weighting for real-time applications // Optics Communications. 2013. № 286. Pp. 111–116. DOI: 10.1016/j.optcom.2012.09.011.

29. GISGeography. Inverse Distance Weighting (IDW) Interpolation. [Электронный ресурс]. URL: https://gisgeography.com/inverse-distance-weighting-idw-interpolation/ (дата обращения: 25.08.2019).

Контактные данные:

Елбек Бахитович Утепов, +7(700)2101733; utepov-elbek@mail.ru

Алексей Анискин, +3(8592)3049406; aaniskin@unin.hr

Азамат Ибрашов, +7(701)7676673; a.ibrashov@csi.kz

Асель Тулебекова, +7(701)6481866; krasavka5@mail.ru